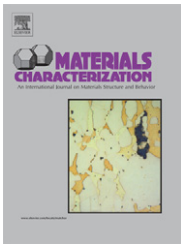

Austenite grain size in the continuous casting process: Metallographic methods and evaluation

J. Reiter[a,*], *C. Bernhard*[a], *H. Presslinger*[b]

[a]*Christian Doppler Laboratory of Metallurgical Fundamentals of Continuous Casting Processes, University of Leoben, Franz-Josef-Straße 15, 8700 Leoben, Austria*
[b]*Voestalpine Stahl GmbH, VOEST-ALPINE-Straße3, 4031 Linz, Austria*

ARTICLE DATA

Article history:
Received 6 November 2006
Received in revised form
5 June 2007
Accepted 8 June 2007

Keywords:
continuous casting
prior-austenite grain size
etching techniques
grain size distribution

ABSTRACT

Austenite grain size is an important parameter for the ductility of steel at elevated temperatures. Therefore, indirect measurements of austenite grain size on slab samples and a specimen from laboratory experiments were carried out. To reveal the prior austenite grain boundaries three etchants (picric acid, ammonium persulfate and nital 3%) were used. One of the main objectives of the present work was to investigate how far the grain size distribution in the specimen from the laboratory experiment corresponds with the grain size distribution on – and beneath – the surface of a continuously cast slab. The measured grain size distribution of a slab and a laboratory experiment – both with an equivalent carbon content of 0.21 wt.% – show a good agreement. A clear maximum grain size can be found for a carbon equivalent of between 0.15 and 0.17 wt.%. The results of the presented metallographic examinations serve as an important basis for the development of an austenite grain growth model.

1. Introduction

The control of the austenite grain size not only plays an important role in rolling, forging or heat treatment but also in the continuous casting process. The formation of transverse cracks during the continuous casting process is generally associated with a low-ductility temperature range due to the formation of precipitates, phases or segregates during cooling that are particularly detrimental along austenite grain boundaries. Due to the decreasing specific grain boundary area, the associated increase of the density of precipitates along the grain boundaries and the sliding of fewer triple points, coarser austenite grains will result in a reduced ductility within the second ductility trough [1–6]. Therefore, the austenite grain size is an important parameter for the ductility, but data regarding the continuous casting process are rare. However, the main influencing parameters are known [4,7–9]:

- steel composition and the corresponding starting temperature for austenite grain growth and the
- thermal cycle during and after solidification.

In a fundamental work, Yasumoto et al. and Maehara et al. [7,9,10] identified an equivalent carbon content of 0.17 wt.% as the composition related to the highest starting temperature for austenite grain growth and the largest austenite grains for cooling rates between 0.1 and 1.5 °C/s. This result was later confirmed by other researchers, e.g. [11].

The influence of nitride and carbonitride forming elements on the final grain size highly depends on the thermal cycle. The higher the temperature and the lower the grain size, the

* *Corresponding author*. Tel.: +43 3842 42189 24; fax: +43 3842 42189 22.
E-mail address: juergen.reiter@mu-leoben.at (J. Reiter).

1044-5803/$ – see front matter © 2007 Elsevier Inc. All rights reserved.
doi:10.1016/j.matchar.2007.06.003

higher is the resultant grain boundary mobility. During continuous casting a specific volume element at the surface remains relatively long – depending on the cooling conditions – at temperatures above the equilibrium precipitation temperature of most nitrides. During this time, the austenite grain rapidly achieves a mean grain diameter of several hundred microns and more, and the related growth rate decreases reciprocally. Together with the reduced grain boundary mobility at lower temperatures this results in an already marginal further growth of the grains, when precipitations along austenite grain boundaries would retard a further growth by pinning effects.

The initial cooling of the strand surface in the continuous casting process therefore plays a decisive role for the austenite grain growth. In order to simulate these thermal boundary conditions under laboratory conditions, an experiment was developed, and several test series on different steel grades were performed in order to investigate the influence of steel composition on austenite grain size. Details of the development of the experiment, the validation of the results and a numerical grain size prediction model were recently published [12]. The present work addresses the metallographic methods which were adopted and partly further developed in order to determine the prior austenite grain size and the grain size distribution at the surface of continuously cast slabs and the specimen from the laboratory experiments. The results of the metallographic examinations are presented and briefly discussed as to their relevance for the validation of the numerical grain size prediction model.

2. Experimental Procedures

The laboratory experiment for the in-situ observation of austenite grain growth under conditions close to the continuous casting process is based on the principle of the so-called Submerged Split Chill Tensile (SSCT)-test [13–16]. The principle of the SSCT-test is schematically presented in Fig. 1: a steel cylinder with a diameter of 58 mm is submerged in a steel melt in an induction furnace. The steel cylinder is spray-coated with zirconium-oxide. The thickness of the coating adjusts the cooling conditions to simulate the process. For the present test series, the cylinder was coated with 0.4 mm zirconium oxide according to the cooling conditions in a slab casting mold. In the SSCT-experiment the solidifying shell is subjected to tension and the tensile force is recorded. The method proved to be valuable for the characterization of the crack susceptibility of steels during solidification. The present experiment has been performed without tensile test: After 30 s of solidification the cylinder and the solidified shell emerge and cool down in air. An increase of the cooling rate by the use of spray water cooling is possible but will not be addressed in this work. The coating thickness of 0.4 mm results in an integral heat flux of 1.2 MW/m^2 over the first 30 s of solidification, similar to a slab casting mould and low casting speed. The temperature increase inside the substrate is monitored by two thermocouples, oppositely positioned and located 2.4 mm beneath the surface. The temperature inside the solidifying shell is also monitored via a thermocouple in a distance of 1 mm from the substrate/shell interface. This temperature only gives a qualitative indication for the cooling conditions, as even the very small diameter of a thermocouple disturbs the sensitive heat balance near the interface. A fourth thermocouple, located in a distance of 17 mm from the surface, allows the monitoring of the superheat of the melt before the start of the solidification experiment. The two measured temperatures inside the substrate allow the prediction of the heat flux at the substrate/shell interface. The heat flux serves as the boundary condition for a solidification model. Shell growth and temperature distribution in the solidifying shell and during the subsequent cooling in air are calculated. A typical cooling curve for a volume element at a distance of 1 mm from the substrate/shell interface is presented in Fig. 2. The superheat of the melt before dipping the substrate is adjusted to between 20 and 30 °C. After cooling to room temperature, the solidified shell is cut into 16 pieces.

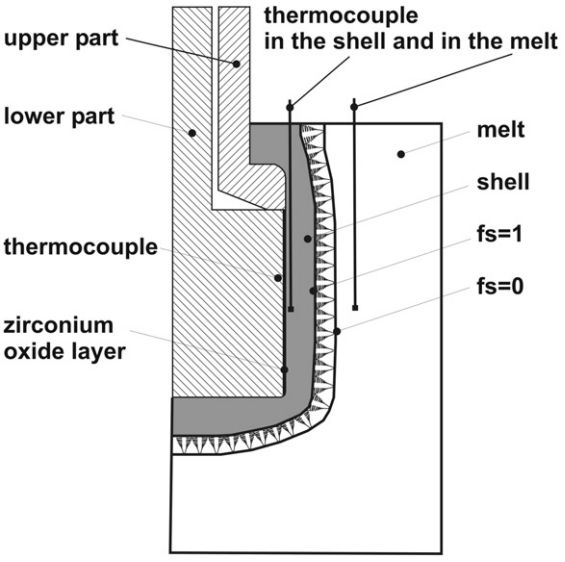

Fig. 1 – Cross section of the test body within the induction furnace, the solidifying steel shell (fraction of solid fs = 0 and fs = 1 corresponds to liquidus and solidus temperature, respectively) and the position of the thermocouples.

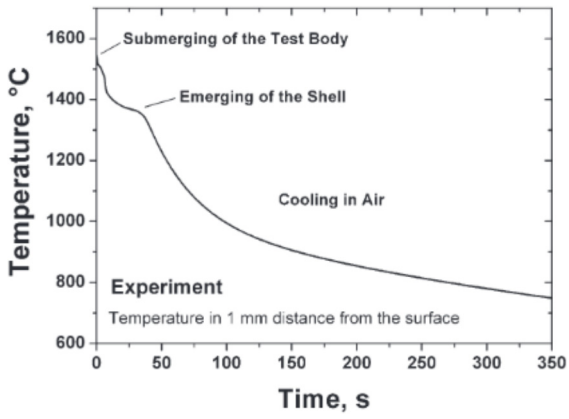

Fig. 2 – The calculated temperature at 1-mm distance from the surface of the shell as a function of time for the experiment with subsequent cooling in air.

Table 1 – Chemical composition, measured mean grain size of the experiment

Test	C, wt.%	Si, wt.%	Mn, wt.%	Mean grain size, mm^2
A1	0.15	0.21	0.31	1.31
A2	0.15	0.21	0.30	1.35
A3	0.45	0.18	0.30	0.23
A4	0.37	0.19	0.38	0.24
A5	0.40	0.19	0.32	0.32
B1	0.05	0.25	1.44	0.36
B2	0.10	0.26	1.46	0.77
B3	0.20	0.26	1.45	0.50
B4	0.51	0.27	1.45	0.15
B5	0.15	0.21	1.04	1.31
B6	0.16	0.22	1.88	0.77
B7	0.08	0.30	1.36	0.83
B8	0.12	0.28	1.34	0.97
B9	0.51	0.29	1.28	0.13
B10	0.70	0.25	1.34	0.11

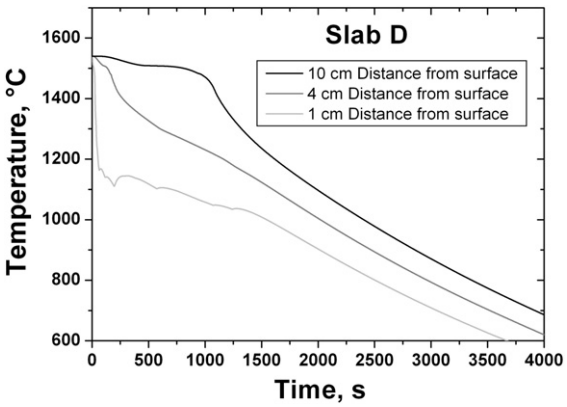

Fig. 3 – Temperature of slab D at different distances from the surface.

Each of these pieces is prepared for metallographic examination and the austenite grain size is determined using a method described in the following section.

The present work presents the results of two test series, both performed on steel with varying C-content. The first one (tests A1–A5) with a Mn-content of between 0.30 and 0.38 wt.% and the second one (tests B1–B10) with between 1.04 and 1.88 wt.% Mn. The composition of these steels and the measured average grain size is given in Table 1.

In order to benchmark the results of the laboratory experiments, the grain size on the surface and at defined distances from the surface was measured for several continuously cast slabs. Chemical composition and casting parameters can be taken from Table 2. The associated solidification and the evolution of the temperature along the surface was calculated with a solidification model. The temperature-time evolution at a distance of 10, 40 and 100 mm from the surface is illustrated in Fig. 3 for the casting parameters of slab D. This figure also underlines what has already been outlined above: assuming a typical equilibrium precipitation temperature of 1050 °C for AlN for an Al-killed steel results in a time period of about 20 min for unhindered austenite grain growth for a grain at a distance of 10 mm below the surface and an even longer time for an increasing distance. After 20 min, the grain growth has already come to an end, and the pinning effect of precipitates therefore does not play an important role for the final grain size. From Fig. 3 it also becomes clear that the different temperatures result in an increasing mean grain size with increasing distance from the surface.

Table 2 – Chemical composition and casting parameter of the slabs

Steel	C, wt.%	Si, wt.%	Mn, wt.%	Casting speed, m/min	Slab thickness, mm	Slab width, mm
A	0.17	0.21	1.50	1.2	215	1294
B	0.19	0.22	0.69	1.2	215	1300
C	0.53	0.24	0.86	1.2	215	1171
D	0.21	0.22	1.45	1.2	215	1406

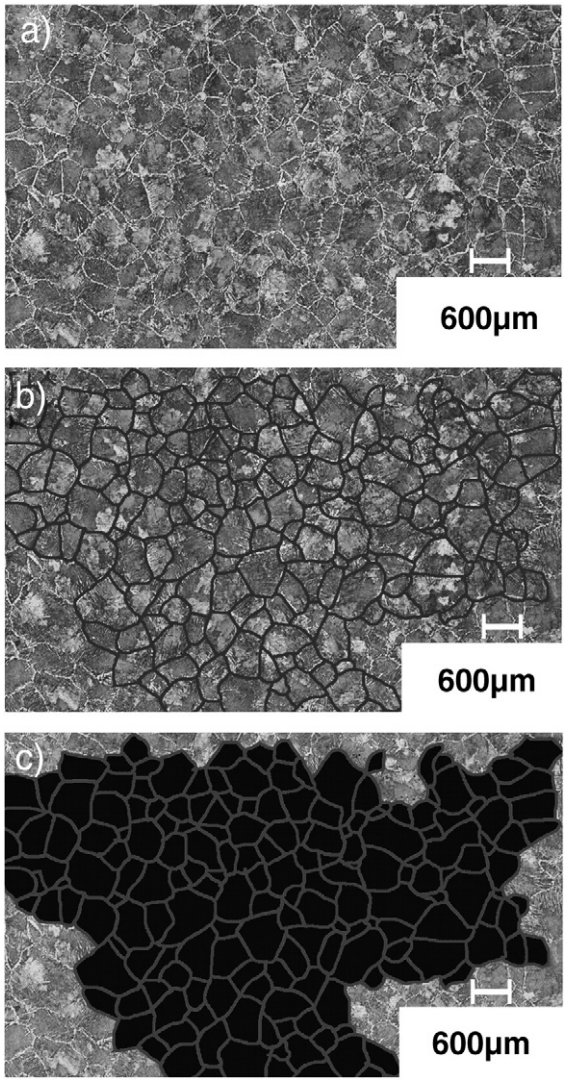

Fig. 4 – Evaluation of the austenite grain size from the micrograph (experiment, 0.4 wt.% C, 1 mm depth) etched with nitric acid in alcohol. (a) A part of an etched micrograph, (b) the manually traced austenite grain boundaries and (c) the image software has identified the grains.

3. Metallographic Work

The standards for the determination of grain size are set in ASTM E112 [17] and DIN EN ISO 643 [18]. There are three distinct methods for the determination of grain size: the comparison procedure, the intercept procedure and the planimetric procedure.

The *comparison procedure* is based on the comparison of three indiscriminate fields of vision per sample with standard series. Repeatability and reproducibility of comparison chart ratings are generally ±1 grain size number. In most cases, a standard magnification of 100× is used for the comparison.

The *intercept procedure* involves an actual count of the number of grains intercepted by a test line. The total length divided by the number of intercepted grains provides the mean intercept length of the grains. This method has commonly been used for the determination of the mean austenite grain diameter, as it is relatively time saving [19].

The third method is the *planimetric (or Jeffries') procedure*. Inside a circle with known area the grains are counted. Grains which are cut from the circle are counted as one half. After conversion to grains per mm^2 the grain size is read from a table.

Using the standardized procedures allows the determination of a grain size number or the mean grain size. However, limitations with respect to the determination of a grain size distribution exist. One of the main objectives of the present work was to investigate how far the grain size distribution in the specimen from the laboratory experiment corresponds with the grain size distribution on – and beneath – the surface of a continuously cast slab. Therefore a more time-consuming method was chosen: The entire polished and etched cross-section (18×70 mm^2 for the slab specimen) was captured by a digital image analysis system in the form of a mosaic of up to 52 single micrographs. The grain size is hence evaluated from areas where a network of coherent grains is clearly visible, since the counting of single non-coherent grains would involve the danger of neglecting small grains. The prior austenite grains are then marked by hand.

Fig. 4 shows a part of a micrograph (etchant nital) with clearly visible prior austenite grain boundaries at different stages of the grain size analysis. The bright phase on micrograph a) is pro-eutectoid ferrite, formed during the γ/α transition, and thus characterizing the austenite grain size near the A_3 temperature. The amount of pro-eutectoid ferrite changes with carbon content and cooling conditions. As can be seen in Fig. 5 the pro-eutectoid ferrite decreases with increasing carbon content. In this case the calculations are carried out with a temperature gradient of 2 °C/s. The equivalent carbon content was derived following the approach of Howe [20].

$$c_p = wt.\%C + 0.14\,wt.\%Si + 0.04\,wt.\%Mn \quad (1)$$

Concerning high equivalent carbon contents little ferrite is visible along the austenite grain boundaries therefore the etching result is not that clear. If a high amount of ferrite is obtained (i.e. low carbon contents), a lot of ferrite grains can be found in the micrograph therefore the contrast differences between grain boundaries and the grain are hence not optimal. It can be concluded that the best etching results can be obtained in a carbon rage of 0.15 to 0.6 wt.% C. In Fig. 4b, the micrograph is overlaid with the network of the manually drawn grain boundaries. Finally, the digital image analysis software has identified the single grains (Fig. 4c). Grains found on the border of the micrograph are not counted. The size of each grain is stored in a table, which is further processed by statistical software. Based on this measurement, the parameters for the most suitable statistical distribution and the mean grain size can finally be calculated.

The preparation of the specimen and the selection of a suitable etchant in order to reveal the prior austenite grain boundaries proved to be the most challenging step in this procedure. In the following, the applied methods are therefore described in detail.

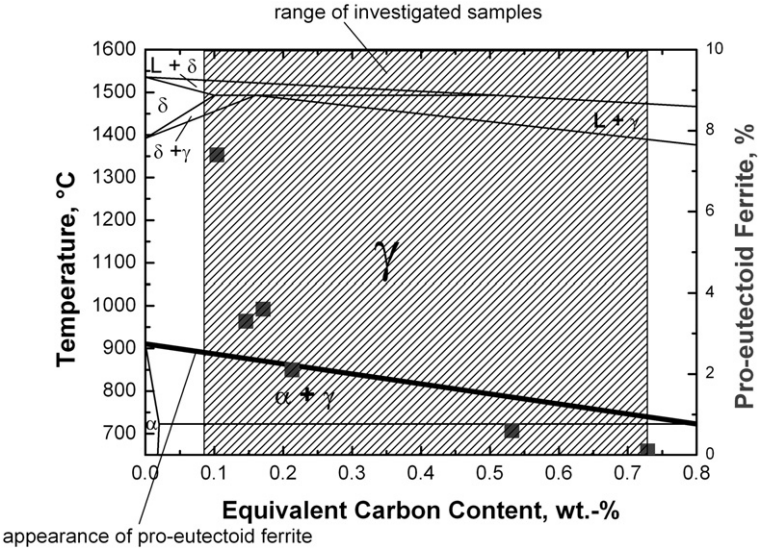

Fig. 5 – Schematic Fe–Fe3C diagram with the range of investigated samples together with the amount of pro-eutectoid ferrite (squares) as a function of the equivalent carbon content.

The determination of the austenite grain size on and beneath the surface of the continuously cast slabs was carried out on 18×70 mm^2 large cross sections, cut off parallel to the surface and 400 mm off the corner on the broad face. Micrographs were prepared in 10 mm steps, starting at the surface and ending in the middle of the slab (Fig. 6a).

The solidified samples from the solidification experiments were cut into 16 pieces (Fig. 6b). Fig. 7 shows the microstructure parallel to the dendrite growth direction. The thickness of the shell amounts to only between 10 and 15 mm. The microstructure corresponds to the near surface zone of a cast slab: the more or less equiaxed characteristic near the surface changes into a columnar structure after a few millimeters. The grain size increases with increasing distance to the interface. The fine grained equiaxed structure on the right-hand side forms during the emergence of the only partly solidified mushy zone. The accelerated cooling prevents the further growth of the grains. This zone cannot be found in a cast product, but provides an insight into the mechanism of the formation of the first austenite grains from a dendritic structure. The austenite grain size is determined on micrographs perpendicular to this plane, and at a distance of 1 mm from the interface as the initial cooling conditions correspond to the casting process and the prior austenite grain boundaries are easier to reveal compared with the interface.

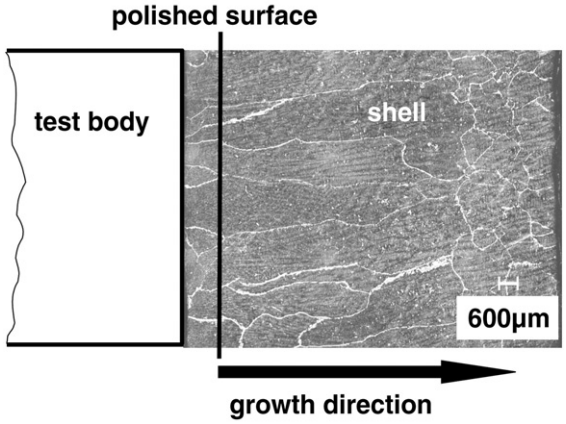

Fig. 7 – Microstructure of the solidified shell (experiment), nital etching.

The most difficult step in the preparation of the samples is the revealing of the prior austenite grain boundaries. Many

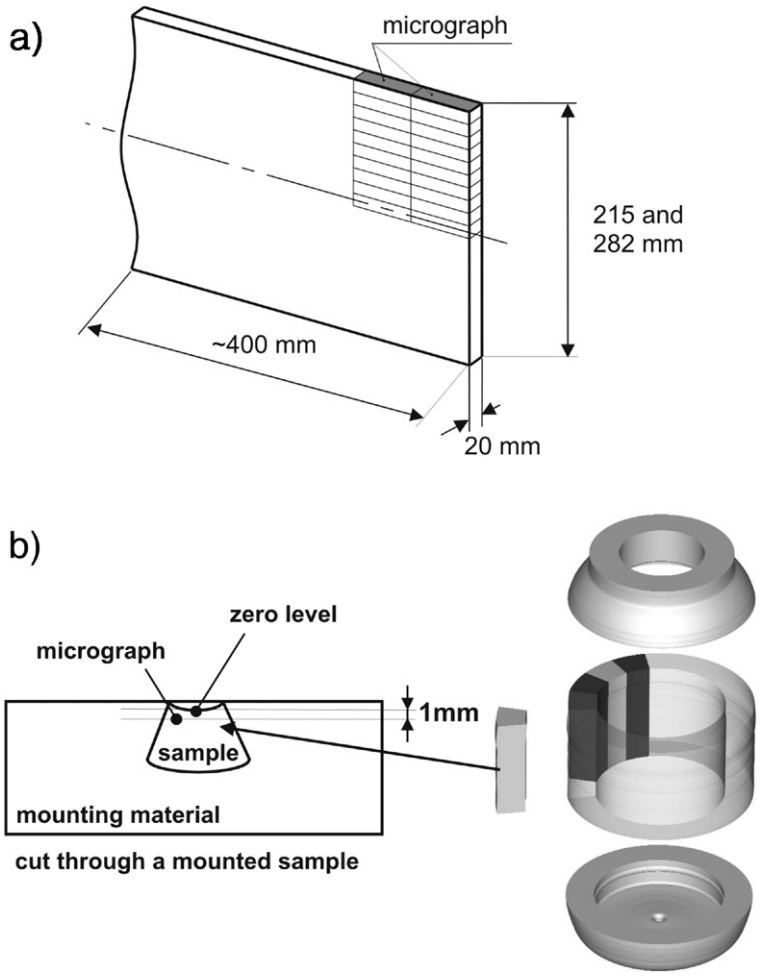

Fig. 6 – (a) Sampling of a slab in 10 mm steps, starting at the surface and ending in the middle of the slab and (b) sampling of the solidified shell from the laboratory experiments (steel shell cut into 16 pieces and mounted).

Table 3 – Etchants to reveal austenite grain size [21,22,25]

(1) Picric acid	170 ml picric acid 30 ml H_2O distilled 6 ml Agepon 1.6 ml HCl after heating up to 50–70 °C etching time between 2 and 5 min
(2) Ammonium persulfate	10 g ammonium persulfate 100 ml H_2O distilled approximate etching time: 5 s
(3) nital 3% (nitric acid in alcohol)	100 ml ethanol 96% 3 ml nitric acid 65% approximate etching time: 5 s

techniques can be found in the literature [21–23]. One of these techniques is to etch the samples with or without pretreatment (e.g. carburisation or oxidation). It should be noted that in the present work numerous samples were analysed. Therefore, a further intention was to save time on metallographic work by finding etchants which demand no pretreatment of the specimen.

In the literature [24–31] different etchants for revealing the prior grain boundaries can be found. A key parameter is the chemical composition of the steel. Moreover it is well known that even minor variations in the composition of the etchant or the etching temperature and time might influence the results. The most frequently used etchant is picric acid together with hydrochloric acid (HCl). Small changes in the proportion of HCl in the solution may change the effect of the etchant. Agepon is a wetting agent that produces wetting of the sample by degreasing the cohesion within the etchant. This leads to a uniform etching result. Picric acid has to be heated up to approximately 60 °C and requires careful handling because of its toxicity. Because of this restriction other etchants such as ammonium persulfate and 3%-nital etchant were investigated. The composition of the etchants is specified in Table 3.

Fig. 8 presents micrographs of steels with different carbon content etched with ammonium persulfate. For an equivalent carbon content of 0.15–0.6 wt.% the best visibility of the former austenite grain boundaries can be obtained. The indicator for

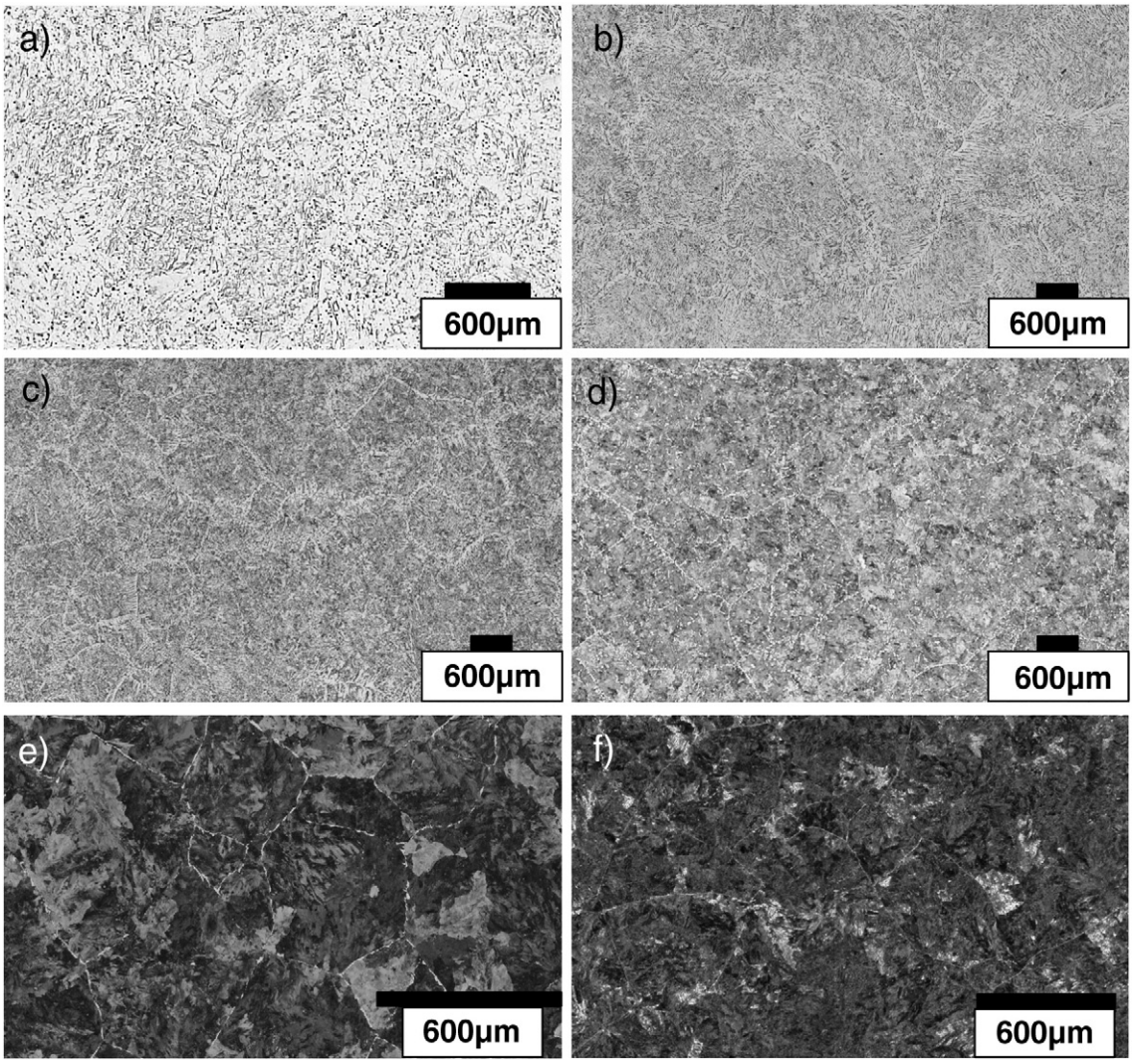

Fig. 8 – Difference in the visibility of austenite grain size over different c_p content, (etchant: ammonium–persulfate). (a) c_p = 0.11 wt.%, (b) c_p = 0.15 wt.%, (c) c_p = 0.18 wt.%, (d) c_p = 0.31 wt.%, (e) c_p = 0.53 wt.% and (f) dark field image c_p = 0.73 wt.%.

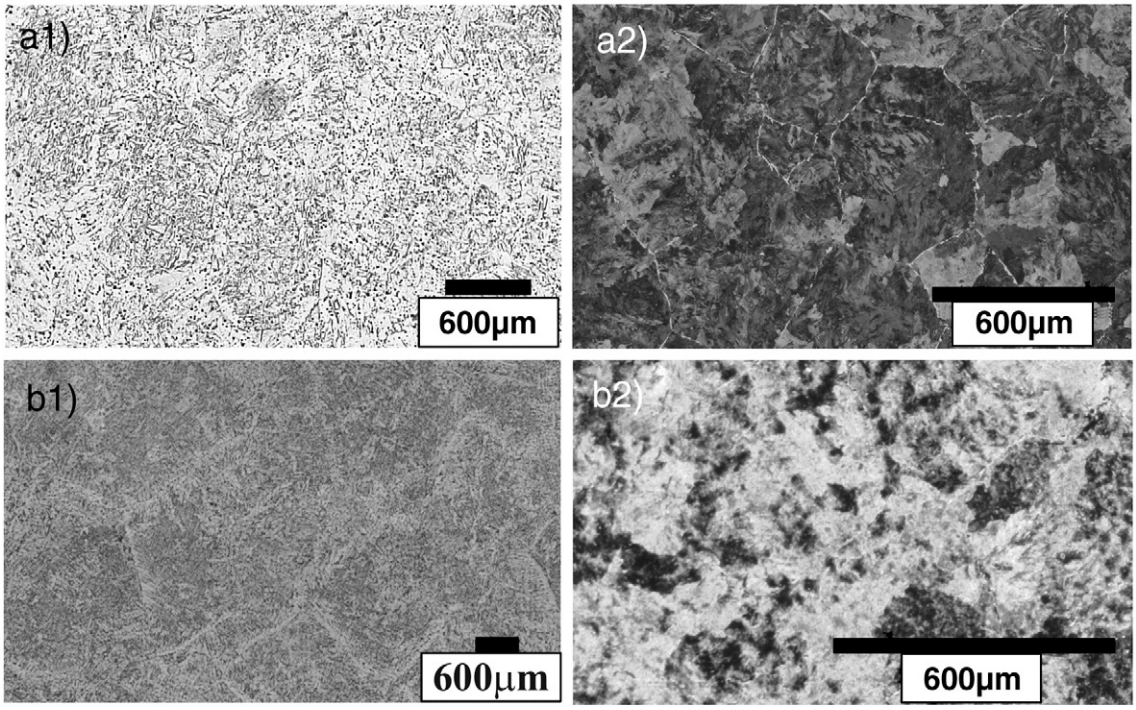

Fig. 9 – Comparison between ammonium persulfate and picric acid on SSCT samples. (a1) Ammonium persulfate, c_p = 0.11 wt.%, (b1) picric acid, c_p = 0.11 wt.%, (a2) ammonium persulfate, c_p = 0.53 wt.%, (b2) picric acid, c_p = 0.53 wt.% (dark field image).

the existence of a former austenite grain boundary is the border-like bright pro-eutectoid ferrite, formed during the γ/α transition. The amount of pro-eutectoid ferrite is – under the given cooling conditions – too high in the case of steels with below 0.15 wt.% C and too small in the case of high carbon steels with more than 0.6 wt.% C (Fig. 8f).

A comparison of two etchants (ammonium persulfate and picric acid) is presented in Fig. 9. In most cases picric acid shows a better etching result for lower carbon content (b1) whereas ammonium persulfate leads to better results for higher carbon content (a2). In addition, alloying elements such as Mn influence the etching result. It should be noted that the dark field microscopy is sometimes a further tool for the improvement of the results. The advantages of ammonium persulfate and nitric acid are their uncomplicated production and handling.

After describing the applied methods for revealing the prior austenite grain size over a wide range of carbon contents, the following section will address the results of the grain size measurement.

4. Results and Discussion

The austenite grain growth is strongly influenced by the thermal history. With increasing distance from the slab surface, the residual time in the existence range of austenite increases too. This results in a coarsening of the grains with increasing distance from the surface. The influence of the increasing initial austenite grain size, caused by the coarsening of the solidification structure is not considered in this context.

Fig. 10 shows two micrographs of slab A with a carbon content of 0.17 wt.% C at distances of 10 and 90 mm from the surface and the same magnification. The coarsening of the grains is obvious.

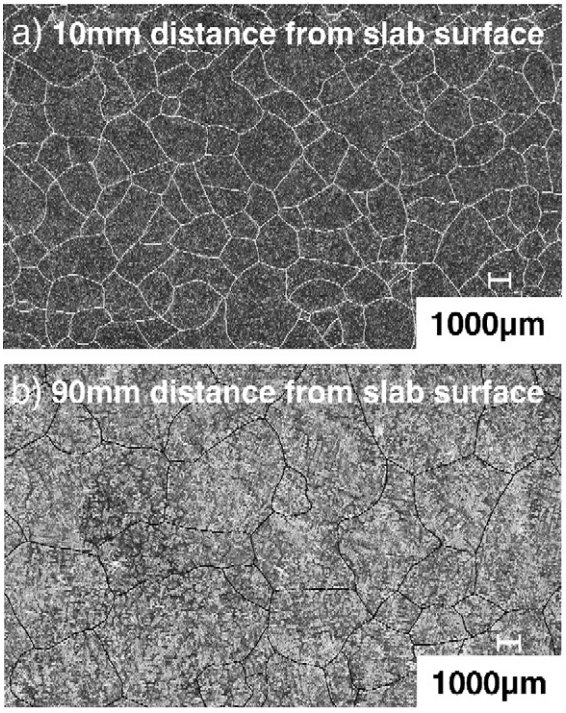

Fig. 10 – Austenite grain size at two different distances from the slab surface for slab A with 0.17 wt.% C (etchant: ammonium persulfate) with traced grains (a) in 10 mm from the slab surface and (b) in 90 mm from the slab surface.

Fig. 11 presents the results of the measurement of the mean austenite grain size for the four investigated slabs versus the distance from the slab surface.

The carbon content of the slabs A, B and D ranges between 0.17 and 0.21 wt.% C. This is, as previously pointed out, the range of carbon content which is expected to show the maximum austenite grain size under similar cooling conditions. In fact, the 0.53 wt.% carbon steels shows a clearly smaller grain size. This confirms that the results of former laboratory experiments are also valid for the continuous casting process [11].

The measured grain size shows the same characteristic trend for all slabs: an increase to a maximum at approximately 90 mm distance from the slab surface and a subsequent decrease towards the center of the slab, according to the dwell time in the austenite region as a function of the distance from the slab surface. The similar cooling conditions for the slabs A, B and D result in rather small deviations of the measured grain size.

After the verification of general tendencies, the next step was to investigate the influence of steel composition and cooling conditions on the austenite grain growth under the well defined laboratory testing conditions.

The entire results of the experimentally determined grain size in the c_p range from 0.07 up to 0.72 wt.% is presented in Fig. 12.

The maximum of the measured mean grain size is found between a c_p of 0.15 and 0.17 wt.%, which corresponds to the findings from the literature [8,32]. Above an equivalent carbon content of 0.17 wt.% the mean grain size decreases with increasing c_p. The influence of Mn on grain size seems to be well explained by the equivalent carbon content as no significant difference between series A and B is in evidence. In addition to the experimental results, the measured grain size at the slab surface is illustrated, underlining the correspondence of process and laboratory simulation.

A further important point concerning the comparability of process and experiment is the grain size distribution. Due to the requirement of nearly identical cooling conditions of the process and the experiment, the grain size distribution can be used to compare the results of the experiment and the process. Fig. 13 shows this comparison for an equivalent carbon content of 0.21 wt.% (Slab A and test B6). As already mentioned before, the austenite grain size of the slab was measured on the surface, while the austenite grain size determined by the experiment was measured 1 mm below the surface. However, the grain size from the surface to 1 mm below the surface of the experiment and the process is nearly constant. Therefore, the comparison of the experimental results and the measured grain size at the slab surface is absolutely feasible. The mean grain size amounts to 0.76 mm^2 for slab A and 0.77 mm^2 for test B6 respectively.

Moreover, the illustrated distribution of the grain size corresponds to a Log-normal distribution, not only near the surface, but also in the middle of the slab. Fig. 14 shows the grain size distribution for three different distances from the surface for slab D and the estimated Log-normal distribution. In Fig. 15 a probability–probability (P–P) plot is used to estimate whether the given data set fits to a specified distribution. Since the values correlate very well, it can be concluded that the values follow a Log-normal distribution. In the figure the

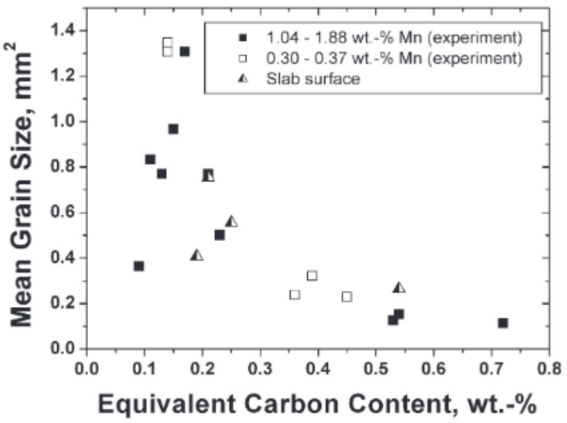

Fig. 12 – Experimentally determined mean austenite grain size vs. equivalent carbon content for steels with two different Mn contents from the laboratory experiment and the results of the measurement of a slab [12].

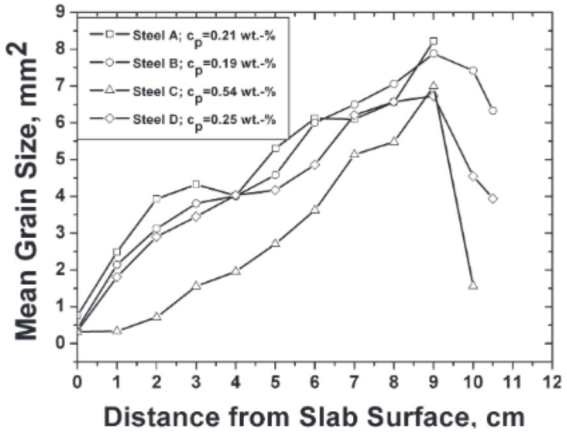

Fig. 11 – Mean austenite grain size of the slabs at varying distances from the surface.

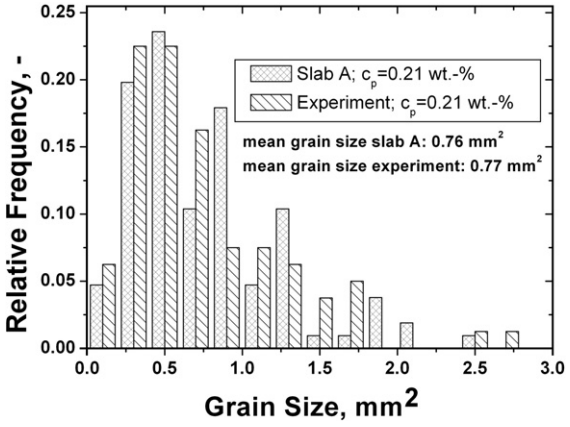

Fig. 13 – Comparison between the grain size of a slab (0 mm depth) and an SSCT test (1 mm depth).

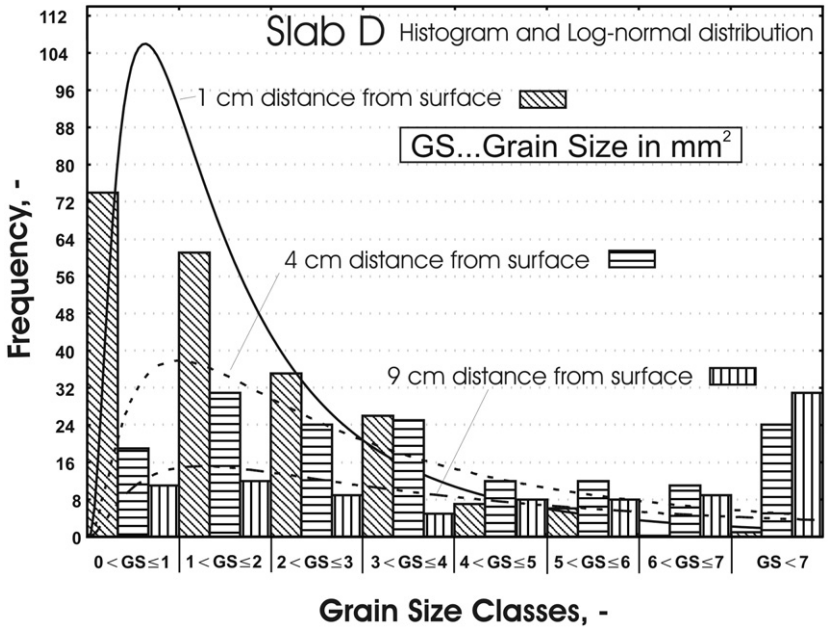

Fig. 14 – Histogram and Log-normal distribution of slab D in different distances from the surface.

values in 1 cm distance below the slab surface are presented. The increasing proportion of large grains with increasing distance from the surface is obvious.

As already pointed out, the results presented here were the basis for the validation of an austenite grain size prediction model, which was recently published [12].

5. Conclusion

(1) The prior austenite grain boundaries were revealed by use of different etchants, namely picric acid, nital etching and ammonium persulfate. The composition of the etchants as well as the etching time and temperature were varied in order to optimize the etching result over a wide range of carbon contents. The metallographic results provide the basis for the determination of a grain size distribution and a mean grain size.

(2) A laboratory experiment was designed in order to simulate the cooling conditions during the initial solidification in the mold, and in order to suppress the precipitation of nitrides and carbonitrides during the subsequent cooling to room temperature.

(3) Additionally, austenite grain sizes from continuously cast slabs were determined. The austenite grain size over the cross section of a slab corresponds to the

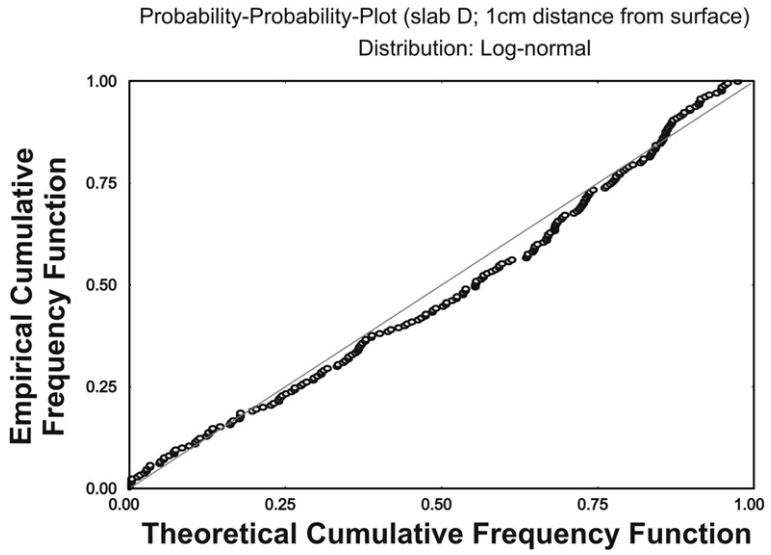

Fig. 15 – Probability–Probability-Plot (Log-normal Distribution) for slab D in 1 cm distance from the surface.

respective dwell time at high temperatures in the purely austenite phase region. After an almost linear increase of the grain size with increasing distance from the slab surface, the grain size reaches a maximum at 90 mm below the surface, and decreases further towards the center of the slab.

(4) The comparison of the results for the slab surface and the laboratory experiment specimen demonstrate the transferability of the experimental results to the continuous casting process. A clear maximum grain size can be found for a carbon equivalent of 0.15–0.17 wt.%. Aside from this maximum, both an increasing and decreasing carbon content results in the formation of finer grains. In further projects the measured austenite grain size can be used as a basis for the adjustment of parameters in a grain size prediction model. Thus the grain size within the second ductility trough at temperatures between 900 and 700 °C can be predicted, allowing a better understanding of the interaction between process conditions and steel composition.

REFERENCES

[1] Schwerdtfeger K. Crack susceptibility of steels in continuous casting and hot forming. Düsseldorf: Verlag Stahleisen; 1994.

[2] Mintz B, Yue S, Jonas JJ. Hot ductility of steels and its relationship to the problem of transverse cracking during continuous casting. Int Mater Rev 1991;36(5):187–217.

[3] Chimani C, Shan GX, Mörwald K, Kolednik O, Böhm HJ, Duschlbauer D, et al. Micromechanical evaluation of intergranular crack growth under continuous-casting conditions. Nice: ECCC; 2005. p. 586–893.

[4] Maehara Y, Yasumoto K, Tomono H, Nagamichi T, Ohmori Y. Surface cracking mechanism of continuously cast low carbon low alloy steel slabs. Mater Sci Technol 1990;6:793–805.

[5] Gomes Maria das Gracas Mendes da Fonseca, de Almeida Luiz Henrique, Gomes Luiz Claudio FC, May Iain Le. Effect of microstructural parameters on the mechanical properties of eutectoid rail steels. Mater Charact 1997;39:1–14.

[6] Deprez P, Bricout JP, Oudin J. Tensile test on in situ solidified notched specimens: effects of temperature history and strain rate on hot ductility of Nb and Nb-V-microalloyed steels. Mater Sci Eng 1993;A168:17–22.

[7] Yasumoto K, Nagamichi T, Maehara Y, Gunji K. Effects of alloying elements and cooling rate on austenite grain growth in solidification and the subsequent cooling process of low alloy steel. Tetsu-to-Hagane (J Iron Steel Inst Jpn) 1987;73 (14):1738–45.

[8] Maehara Y, Yasumoto K. Effect of carbon on hot ductility of As-cast low alloy steels. Trans ISIJ 1985;25:296.

[9] Maehara Y, Tomono H, Yasumoto K. Effect of notch geometry on hot ductility of austenite. Trans ISIJ 1987;27:103–9.

[10] Maehara Y, Yasumoto K, Tomono H, Nagamichi T, Ohmori Y. Surface cracking mechanism of continuously cast low carbon low alloy steel slabs. Mater Sci Technol 1990;6:793–805.

[11] Maehara Y, Yasumoto K, Sugitani Y, Gunji K. Effect of carbon on hot ductility of As-cast low alloy steels. Trans ISIJ 1985;25:1045–52.

[12] Reiter J, Bernhard C, Preßlinger H. Determination of Austenite Grain Size in Relation to Product Quality of the Continuous Casting Process. Materials Science & Technology (MS&T '06), Conference and Exhibition, Cincinnati, USA; October 2006. p. 805–16.

[13] Ackermann P, Kurz W, Heinemann W. In situ tensile testing of solidifying aluminium and Al–Mg-shells. Mater Sci Eng 1985;75:79–86.

[14] Hiebler H, Bernhard C. Mechanical properties and crack susceptibility of steel during solidification. Steel Res 1999;69 (8+9):349–55.

[15] Bernhard C, Xia G. Influence of alloying elements on the thermal contraction of peritectic steels during initial solidification. Ironmak Steelmak 2006;33(1):52–6.

[16] Bernhard C, Hiebler H, Wolf M. Experimental Simulation of Subsurface Crack Formation in Continuous Casting. Rev Métall CIT 2000:333–44.

[17] Annual book of ASTM standards: Section 3, Metals test methods and analytical procedures ; 2002,1; Metals—mechanical testing; elevated and low-temperature tests; metallography.

[18] Steels Metallographic determination of the apparent grain size German Version EN 643:2003.

[19] Giumelli AK, Militzer M, Hawbolt EB. Analysis of the austenite grain size distribution in plain carbon steels. ISIJ Int 1999;39 (3):271–80.

[20] Howe AA. Segregation and Phase Distribution during solidification of Carbon, Alloy and Stainless Steels. EUR 133303. Luxembourg: ECSC; 1991.

[21] Bekert M, Klemm H. Handbuch der metallographischen Ätzverfahren. 3., bearbeitete Auflage. Leibzig: VEB Deutscher Verlag für Gunststoffindustrie; 1976.

[22] Schacht E, Richter J. Erfahrungen mit Ätzmitteln zum Nachweis der ehemaligen Austenitkorngrenzen in Stählen. Prakt Metallogr 1998;35:384–95.

[23] Garcıá de Andrés C, Caballero FG, Capdevila C, San Martín D. Revealing austenite grain boundaries by thermal etching: advantages and disadvantages. Mater Charact 2003;49:121–7.

[24] Petzlow G. Metallographisches, Keramographisches, Plastographisches Ätzen. Materialkundlich-Technische Reihe 1, 6. überarbeitete Auflage. Berlin: Gebrüder Borntraeger; 1994. p. 111–22.

[25] Béchet S, Beaujard L. Nouveau réactif pour la mise en évidence micrographique du grain austénitique des aciers trempés ou trempés-revenus. Rev Metall 1955;10:830–6.

[26] Baldinger P, Posch G, Kneissl A. Pikrinsäureätzung zur Austenitkorncharakterisierung mikrolegierter Stähle. Prakt Metallogr 1991;21:252–61.

[27] Zhang L, Cheng Guo D. A general etchant for revealing prior-austenite grain boundaries in steels. Mater Charact 1993;30:299–305.

[28] Vander Voort GF. Metallography principles and practice. The Materials Information Society; 1999.

[29] Angelica Schrader A, Rose A. De ferri metallographia / Alta Auctoritas Communitatis Europaeae Carbonis Ferrique. Düsseldorf: Verlag Stahleisen 2. Gefüge der Stähle; 1966.

[30] Habraken L, De Brouwer JL. De ferri metallographia / Alta Auctoritas Communitatis Europaeae Carbonis Ferrique. Düsseldorf, Verlag Stahleisen 1. Grundlagen der Metallographie;1966.

[31] Garcıá de Andrés C, Bartolomé MJ, Capdevila C, San Martín D, Caballero FG, López V. Metallographic techniques for the determination of the austenite grain size in medium-carbon microalloyed steels. Mater Charact 2001;46:389–98.

[32] Schwerdtfeger K, Köthe A, Rodriguez JM, Bleck W. Thin slab casting, Volume 1, Luxemburg: EUR 19409/1 EN; 2001. p. 33–48.